Geophys. J. Int. (1997) **129**, 29–40

The forward problem of electromagnetic induction: accurate finite-difference approximations for two-dimensional discrete boundaries with arbitrary geometry

Claudia Aprea, John R. Booker and J. Torquil Smith*

Geophysics Program, Box 351650, *University of Washington, Seattle,* WA 98195, *USA. E-mail: booker@geophys.washington.edu*

Accepted 1996 November 12. Received 1996 October 28; in original form 1996 July 11

SUMMARY

We describe finite-difference approximations to the equations of 2-D electromagnetic induction that permit discrete boundaries to have arbitrary geometrical relationships to the nodes. This allows finite-difference modelling with the flexibility normally ascribed to finite-element modelling. Accuracy is demonstrated by comparison with finite-element computations. We also show that related approximations lead to substantially improved accuracy in regions of steep, but not discontinuous, conductivity gradient.

Key words: electromagnetic induction, finite-difference methods.

1 INTRODUCTION

The advent of large accurate magnetotelluric (MT) data sets (e.g. Wannamaker *et al.* 1989; Jones & Craven 1990; Jones *et al.* 1993; Ogawa *et al.* 1996; Chen *et al.* 1996) has accentuated the need to invert such data directly for electrical conductivity structure. A critical requirement, however, is a fast and accurate forward algorithm to calculate the electric and magnetic fields in arbitrary conductivity structures. Existing algorithms generally fall into finite-difference and finite-element approximations to the governing differential equations.

Finite elements involve assumed functional forms for the model and fields in small regions of specified geometry. The fields are then matched where the elements abut. Typically, the elements are triangular, the conductivities are assumed to be constant and the fields are assumed to vary linearly within each triangle (e.g. Rodi 1976; Wannamaker, Stodt & Rijo 1987). Finite elements are generally thought to have the advantage of being able to model complicated structures more easily than finite differences when there are discontinuities.

Finite-difference approximations (FDAs) (Jones & Pascoe 1971; Williamson, Hewlett & Tammemagi 1974; Jones & Thompson 1974; Brewitt-Taylor & Weaver 1976; Adhidjaja & Hohmann 1989), on the other hand, are conceptually simpler, and in their usual implementation lead to sparser matrix equations. The conductivities and fields are sampled at the nodes of a finite grid. The fields between the nodal points are locally approximated using low-degree polynomials determined from the field values at a small number of nodal points (usually five). The field derivatives are estimated by differentiating these polynomials. The conductivity model is assumed to behave between nodes in a way that does not impair the accuracy of approximating the fields by polynomials. However, if the model is anywhere discontinuous, the fields or their spatial derivatives may also be discontinuous and thus poorly approximated by polynomials. In such cases, maintaining accuracy requires special treatment. Furthermore, it is generally believed that discontinuities must coincide with the grid and hence sloping interfaces have typically been simulated using a series of steps. Steps obviously lead to problems for the case of topography, because it becomes very difficult to determine accurately the surface fields tangential to the slope. In this paper, we present FDAs that are as flexible as finite-element approximations in modelling model discontinuities with complex geometry, and we present results demonstrating their accuracy.

We discuss only the 2-D problem. The general ideas are applicable in 3-D, but are complicated by the necessity of defining the electric and magnetic fields on staggered grids to enforce electric current continuity (Mackie, Madden & Wannamaker 1993; Mackie, Smith & Madden 1994; Smith 1996a,b). The vector electric and magnetic fields are denoted by **E** and **H** and their components by appropriate subscripts. The forward problem for 2-D electromagnetic induction then separates into two distinct polarizations: the transverse electric (TE) mode (sometimes called E-parallel, H-perpendicular or E-polarization), in which the electric currents flow perpendicular to the 2-D profile (along strike); and the transverse magnetic (TM) mode (sometimes called E-perpendicular, H-parallel or H-polarization), in which the currents flow along the 2-D profile (perpendicular to strike). We define the strike direction

* Now at: Engineering Geosciences, University of California, Berkeley, CA 94720-1760, USA.

to be x and the 2-D conductivity to be $\sigma(y, z)$. Its reciprocal, the 2-D resistivity, is $\rho(y, z)$. The 2-D profile direction, y, is horizontal and increases to the right; z is vertical and increases downwards. For the TE mode, and a time dependence $\exp(-i\omega t)$, Maxwell's equations in a good conductor plus Ohm's Law reduce to

$$(\nabla \times \nabla \times \mathbf{E})_x = \nabla \cdot \nabla E_x = \nabla^2 E_x = \frac{\partial^2 E_x}{\partial y^2} + \frac{\partial^2 E_x}{\partial z^2} = -i\omega\sigma\mu_0 E_x, \tag{1a}$$

$$\frac{\partial E_x}{\partial z} = -i\omega\mu_0 H_y, \tag{1b}$$

$$\frac{\partial E_x}{\partial y} = i\omega\mu_0 H_z, \tag{1c}$$

where ∇ and ∇^2 are the 2-D gradient and Laplacian. For the TM mode, the equivalent equations are

$$\begin{aligned}(\nabla \times \rho\nabla \times \mathbf{H})_x &= \nabla \cdot \rho\nabla H_x = \rho\nabla^2 H_x + \nabla\rho \cdot \nabla H_x \\ &= \rho\left(\frac{\partial^2 H_x}{\partial y^2} + \frac{\partial^2 H_x}{\partial z^2}\right) + \frac{\partial\rho}{\partial y}\frac{\partial H_x}{\partial y} + \frac{\partial\rho}{\partial z}\frac{\partial H_x}{\partial z} \\ &= -i\omega\mu_0 H_x,\end{aligned} \tag{2a}$$

$$\frac{\partial H_x}{\partial z} = \sigma E_y, \tag{2b}$$

$$\frac{\partial H_x}{\partial y} = -\sigma E_z. \tag{2c}$$

The problem is to find accurate approximations to eqs (1a) and (2a) when the fields are known only on a finite grid. Difficulties arise when σ or ρ are discontinuous, because the second derivatives of the fields in eqs (1a) and (2a) may be discontinuous and then Laplacian terms in the above equations are not well defined. The TM-mode approximation at a discrete boundary is somewhat more difficult than the TE, because the unbounded first derivative of ρ enters directly in eq. (2a).

Eqs (1b, c) or (2b, c) are used only to calculate the auxiliary fields H_y and H_z or E_y and E_z once the primary fields E_x or H_x have been determined by solving the approximations to eqs (1a) and (2a) with appropriate boundary conditions. These auxiliary fields are easier to measure in the field than are the spatial derivatives of the primary fields. For instance, 2-D MT assumes that the measured horizontal electric and magnetic fields at the Earth–air interface in the frequency domain are related by

$$\begin{bmatrix} E_x \\ E_y \end{bmatrix} = \begin{bmatrix} 0 & Z_{xy} \\ Z_{yx} & 0 \end{bmatrix} \begin{bmatrix} H_x \\ H_y \end{bmatrix}.$$

The off-diagonal impedances, $Z_{xy} = E_x/H_y$ and $Z_{yx} = E_y/H_x$ correspond to the TE and TM modes. These are commonly transformed to the MT responses:

Apparent Resistivity $\quad \rho_{ij} = \dfrac{1}{\omega\mu_0}|Z_{ij}|^2,$

Impedance Phase $\quad \phi_{ij} = \arg[Z_{ij}].$

2 FDA FOR THE TE MODE

When the electric field and its derivatives are continuous, one can accurately approximate the field locally from its values at nodal points using an interpolating polynomial. The degree of this polynomial must be at least as high as the derivatives in the equations to be approximated and will require information from fewer nodes if the degree is kept low. The most commonly used approximation for the Laplacian on the left side of eq. (1a) uses a second-degree polynomial, which requires values from only the four nodes surrounding the node at which the equation is approximated. Differentiating the interpolating polynomial leads to estimates of the required derivatives in terms of the nodal values and hence the FDA. Although the electric field and its first derivatives are everywhere continuous for the TE mode, the second derivatives can jump across surfaces where σ is discontinuous. Even when σ is continuous inside the model, the second derivatives of the electric field may be discontinuous at the Earth–air interface. Polynomial approximation of the field at such discontinuities will necessarily lead to inaccurate estimates of the Laplacian.

To see what to do when the conductivity is discontinuous, consider a typical nodal point 'O' in a rectangular, but not necessarily uniform, grid. Its neighbouring nodes are R (right), L (left), U (up) and D (down), which are respectively located at distances Δ_R, Δ_L, Δ_U and Δ_D from O (see Fig. 1). Let O also be a point at which eight abutting triangular regions of (possibly different) conductivity meet as shown. Now integrate eq. (1a) over the rectangular area A in Fig. 1, whose sides intersect the grid halfway between O and each of the adjacent nodes. Gauss' Theorem can be used to transform the area integral on the left-hand side to an integral around the perimeter of A:

$$\int_A (\nabla \cdot \nabla E_x)\, dA = \int (\hat{\mathbf{n}} \cdot \nabla E_x)\, dl, \tag{3}$$

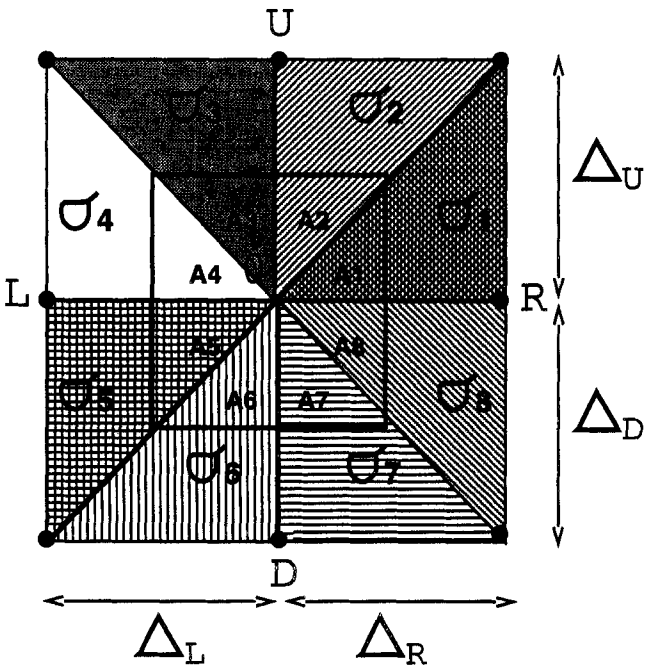

Figure 1. Nodal point O in a rectangular grid at which eight abutting triangular regions of potentially different conductivities σ_i meet. The A_i are the areas of each triangle with a rectangular region of total area $A = \Sigma A_i$ that extends halfway to the adjacent nodes.

where $\hat{\mathbf{n}}$ is the outward unit normal to the edges of A. Since the first derivatives of E_x are everywhere continuous, we can accurately approximate derivatives normal to the contour of integration in (3) using centred first differences. For instance, along the right edge of A we have

$$\int \frac{\partial E_x}{\partial y}\, dl \approx \left(\frac{\Delta_U + \Delta_D}{2}\right)\frac{E_R - E_O}{\Delta_R}.$$

Adding the contributions from the four sides of A, the contour integral becomes

$$\approx \left(\frac{\Delta_L + \Delta_R}{2}\right)\left[\frac{E_D - E_O}{\Delta_D} - \frac{E_O - E_U}{\Delta_U}\right] + \frac{\Delta_U + \Delta_D}{2}\left[\frac{E_R - E_O}{\Delta_R} - \frac{E_O - E_L}{\Delta_L}\right] + O(\Delta^2), \tag{4}$$

where $E_{O,R,L,U,D}$ are the values of E_x at the nodes O, R, L, U, and D and Δ is a typical node spacing. One can easily show, using the Lagrange interpolation formula (Davis & Polonsky 1964), that the leading error term in (4) becomes identically zero on a uniform grid (see Smith 1988).

The integrated right-hand side of eq. (1a) can be approximated using

$$i\omega\mu_0 \int_A E_y(x, z)\sigma(x, z)\, dA \approx i\omega\mu_0 E_O \int_A \sigma(x, z)\, dA \approx i\omega\mu_0 E_O \sum_{i=1}^{8} \sigma_i A_i + O(\Delta^3), \tag{5}$$

where σ_i are the spatially averaged conductivities in the eight small triangles of area A_i inside A. When σ is non-uniform, the error term that we are neglecting in (5) involves ∇E_x even when the grid is uniform. Since we are keeping terms involving ∇E_x in (4), one needs to check that the neglected term in (5) is substantially smaller than the retained terms in (4). This turns out to require that

$$\frac{|\nabla E_x|\Delta}{\delta^2}\Delta^2 \ll |\nabla E_x|\Delta,$$

where $\delta = \sqrt{2/\omega\mu_0\sigma}$ is an appropriate 'skin depth'. This inequality reduces to $\Delta^2 \ll \delta^2$ and we have the reasonable (and well-known) result that the node spacing must be small compared to the local skin depth. It is a good idea to take advantage of the higher order of accuracy of the FDA on a uniform grid and make the node spacing the same on either side of a discontinuity and a fraction of the skin depth in the most conducting medium. For high-accuracy results, we recommend $\Delta \approx \delta/10$ near the surface of the model. This can be progressively relaxed with depth as the contribution of inaccuracies in the FDA to errors in the surface fields decays. It can also be relaxed in the horizonal away from model (and hence field) gradients. We have found that an effective compromise between keeping the grid uniform and minimizing the number of nodes is to increase each successive node spacing by 10 per cent in the vertical and to increase horizontal spacing by 50 per cent outside regions of uniform nodes where strong lateral variations occur.

Combining (4) and (5) and rescaling the result by dividing by the total area of integration $A = (\Delta_L + \Delta_R)(\Delta_U + \Delta_D)/4$ we finally obtain

$$\frac{2}{\Delta_R + \Delta_L}\left[\frac{E_R - E_O}{\Delta_R} + \frac{E_L - E_O}{\Delta_L}\right] + \frac{2}{\Delta_U + \Delta_D}\left[\frac{E_D - E_O}{\Delta_D} + \frac{E_U - E_O}{\Delta_U}\right] = -i\omega\mu_0\tilde{\sigma}_O E_O, \tag{6a}$$

where the 'effective conductivity' at the central node is defined by

$$\tilde{\sigma}_O \equiv \frac{1}{A}\sum_{i=1}^{8} \sigma_i A_i. \tag{6b}$$

For a uniform grid with nodal spacing Δ and a constant conductivity σ_O, (6a) reduces to

$$\frac{1}{\Delta^2}[E_L + E_R + E_U + E_D - 4E_O] = -i\omega\mu_0\sigma_O E_O. \tag{6c}$$

The left sides of (6a) and (6c) are the standard five-point FDAs for the Laplacian operator on non-uniform and uniform grids.

The result embodied in (6a) and (6b) is particularly simple to implement and can be generalized. The TE FDA in a medium with general conductivity variation is the same as in a medium with constant conductivity, except that nodal values of conductivity must be replaced with effective values that are spatial averages of the actual conductivities around each nodal point out to half the distance to the adjacent nodes. When the conductivity is continuous, this average will commonly be close enough to the actual conductivity at the node that it is not worth bothering about the difference (i.e. just set $\tilde{\sigma}_O = \sigma_O$). However, when the conductivity is discontinuous, the local spatial average that must be assigned to the node will usually be substantially different from the actual value of σ at the node. In practice, one may need a nodal spacing smaller than the skin-depth arguments suggest in order to make the effective conductivities easy to compute. For instance, one would probably always want several nodes within a discrete body. Likewise, nodal spacing in a continuous conductivity variation should be small compared to the scale of the gradient of conductivity.

As a simple example, consider the FSA at a node on a horizontal interface within a uniform grid. Then, $\tilde{\sigma} = 1/2(\sigma_{O+} + \sigma_{O-})$, where σ_{O+} and σ_{O-} are the conductivities just above and below the interface. One gets the same result for a vertical or diagonal interface. Thus, we see that an interface that cuts diagonally across a mesh cell is as easy to model as an interface that is coincident with the mesh.

With the appropriate definition of effective conductivity, (6a) and (6b) should be useful for completely arbitrary boundaries, which may not pass through any nodes. As derived, the first differences in (4) do not span a discontinuity, so that their errors, which involve second derivatives, are always bounded. However, their errors would remain bounded, although they may be larger, even if the first differences do span a model discontinuity. This is because the second derivatives are only discontinuous, not unbounded. Thus running the model discontinuities through node O improves accuracy, but is otherwise a matter of convenience. There is clearly no need to pass the discontinuity through O in the derivation of the right side of the FDA. It is simply necessary to define the effective conductivity so as to weight each constituent σ according to

its area inside A. This involves no degradation in the accuracy of the right side of the FDA.

3 FDA FOR THE TM MODE

3.1 Discontinuous model

A similar approach can be used for the TM mode at a discontinuity. We again look at a node O, at which up to eight triangular regions with (possibly) different resistivities, $\rho_i = 1/\sigma_i$, come together. Integrating (2a) over the same area A used for the TE mode and again using Gauss' Theorem gives

$$\int_A \nabla \cdot \rho \nabla H_x \, dA = \int \hat{\mathbf{n}} \cdot \rho \nabla H \, dl = i\mu_0 \int_A H_x \, dA, \tag{7}$$

where $\hat{\mathbf{n}}$ is the outward unit normal to the edges of A. Since the right side of (7) does not involve ρ, and the magnetic field and its first derivatives are always continuous for the TM mode, we can approximate it by

$$\approx \mu_0 H_O \sum_{i=1}^{8} A_i = \frac{\mu_0 H_O}{4}(\Delta_L + \Delta_R)(\Delta_U + \Delta_D) + O(\Delta^3), \tag{8}$$

where H_O is the value of H_x at O.

The left side of (7) is more complicated than its TE-mode equivalent. The derivatives of H_x normal to the edges of A can again be estimated from centred first differences that do not span discontinuities in ρ or ∇H_x. However, ρ varies along the integration path and it is therefore necessary to use the appropriate ρ_i for each path segment (see Fig. 1). For instance, along the right edge of A, we have

$$\int \rho \frac{\partial H_x}{\partial y} dl \approx \left(\rho_1 \frac{\Delta_U}{2} + \rho_8 \frac{\Delta_D}{2} \right) \frac{H_R - H_O}{\Delta_R} + O(\Delta^2) \tag{9}$$

(again, the subscripts on H denote the node at which H_x is measured). As a result, the FSA does not depend on one 'effective conductivity'. Instead, there are four 'effective resistivities':

$$\tilde{\rho}_R = \frac{(\rho_1 \Delta_U + \rho_8 \Delta_D)}{(\Delta_U + \Delta_D)}, \qquad \tilde{\rho}_L = \frac{(\rho_4 \Delta_U + \rho_5 \Delta_D)}{(\Delta_U + \Delta_D)},$$

$$\tilde{\rho}_D = \frac{(\rho_6 \Delta_L + \rho_7 \Delta_R)}{(\Delta_L + \Delta_R)}, \qquad \tilde{\rho}_U = \frac{(\rho_3 \Delta_L + \rho_2 \Delta_R)}{(\Delta_L + \Delta_R)}, \tag{10}$$

where the $\rho_i = 1/\sigma_i$ are defined in Fig. 1.

The final FDA is

$$\frac{2}{\Delta_R + \Delta_L}\left[\tilde{\rho}_R \frac{H_R - H_O}{\Delta_R} + \tilde{\rho}_L \frac{H_L - H_O}{\Delta_L} \right] + \frac{2}{\Delta_U + \Delta_D}\left[\tilde{\rho}_D \frac{H_D - H_O}{\Delta_D} + \tilde{\rho}_U \frac{H_U - H_O}{\Delta_U} \right] = -i\omega\mu_0 H_O. \tag{11}$$

No special consideration of the FDA is required at the Earth–air interface for the TM mode because the boundary condition H_x = constant is valid at this interface, even in the case of topography. Just as for the TE mode, one can use (11) with degraded accuracy if the discrete boundaries do not pass through O. However, the effective resistivities must be based on the contribution of each constituent resistivity to the integrals along the four edges and are more onerous to calculate. In contrast to the TE mode, the accuracy of the left side of (11) does not improve by one order on a uniform grid unless ρ is also uniform. However, the order of accuracy of the right side does improve on a uniform grid. Comparison of the neglected first-derivative term on the right with the retained first-derivative terms on the left again leads to the requirement that $\Delta_2 \ll \delta^2$.

3.2 Continuous model

The FDA (11) is also valid away from a model discontinuity, but care must be taken in defining the effective resistivities. The simplest approximation, in which the effective resistivities are estimated to be the resistivity at the central node, ρ_O, reduces the left side of (11) to the standard FDA for $\rho \nabla^2 H_x$ and thus ignores the first-derivative terms in (2a). One can restore these terms by approximating them with first differences centred on O. The resultant FDA,

$$2\frac{\rho_O}{\Delta_R + \Delta_L}\left[\frac{H_R - H_O}{\Delta_R} + \frac{H_L - H_O}{\Delta_L} \right] + 2\frac{\rho_O}{\Delta_U + \Delta_D}\left[\frac{H_D - H_O}{\Delta_D} + \frac{H_U - H_O}{\Delta_U} \right] = -i\omega\mu_0 H_O, \tag{12}$$

was used successfully by Smith (1988) and Smith & Booker (1991) in a rapid algorithm for 2-D inversion of MT data.

Alternatively, the resistivity on each segment of the contour integral around the area A can be approximated by linear interpolation between O and the nearest node outside A. The effective resistivities then become

$$\tilde{\rho}_R = \frac{\rho_R + \rho_O}{2}, \qquad \tilde{\rho}_L = \frac{\rho_L + \rho_O}{2},$$

$$\tilde{\rho}_D = \frac{\rho_D + \rho_O}{2}, \qquad \tilde{\rho}_U = \frac{\rho_U + \rho_O}{2}. \tag{13}$$

We call (11), using the effective resistivities (9), the TM(d) FDA; we call (12) the TM(c1) FDA; and we call (11), using the effective resistivities (13), the TM(c2) FDA. We shall see that TM(d) gives excellent results for discrete boundaries and that both TM(c1) and TM(c2) work well for models with modest conductivity gradients. However, TM(c2) performs much better than TM(c1) as the resistivity gradients become large. Obviously, practical estimation of the effective resistivities in all three cases may again require nodal spacings smaller than skin-depth arguments would suggest.

4 EXAMPLES

4.1 The TE mode with topography

If the grid is uniform about a node on the Earth–air interface and we let $\sigma_{O+} = \sigma_{air} = 0$ and $\sigma_{O-} = \sigma_{Earth}$, we find that $\tilde{\sigma} = 0.5\sigma_{Earth}$. Brewitt-Taylor & Weaver (1976) have already suggested this result by making an analogy with the 1-D case, and our derivation shows that it is rigorously justified in 2-D when the node spacing is the same on either side of the interface. More generally, $\tilde{\sigma}$ depends on the ratio of the node spacing on either side of the interface. More complicated shapes for the Earth–air interface, including the possibility of an internal discontinuity intersecting the surface, can easily be constructed using combinations of the triangular regions in Fig. 1. For instance, suppose that the grid is uniform and that

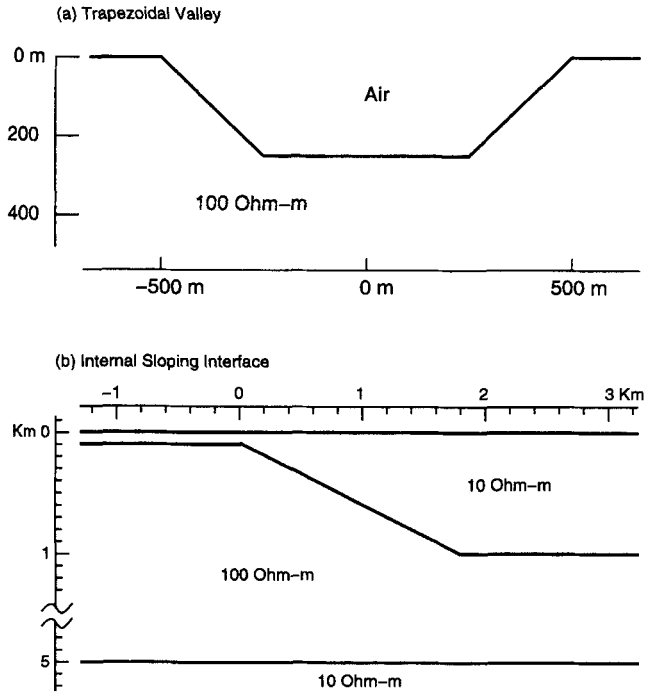

Figure 2. Two models used to compare the accuracy of the finite-difference and finite-element calculations with sloping boundaries. Note the break in vertical scale for model (b).

the interface has a corner at O, with the interface horizontal to the left of O and sloping up at 45° to the right of O. Five of the eight triangles have $\sigma = \sigma_{\text{Earth}}$ and three have $\sigma = 0$. Consequently, $\tilde{\sigma} = 0.625\sigma_{\text{Earth}}$.

As a test, we compare results using (6a) for the trapezoidal valley model shown in Fig. 2(a) with results using the finite-element code of Wannamaker *et al.* (1987). This finite-element code (PW2D) reduces the forward problem to a linear system $\mathbf{Ax} = \mathbf{b}$ in which $\mathbf{A}$ has nine non-zero diagonals. This system is solved by complete decomposition of the matrix $\mathbf{A}$. Our code (FWD2D) reduces the FDA plus the boundary conditions to a linear system in which $\mathbf{A}$ has five non-zero diagonals. The system is solved using an efficient iterative technique that takes advantage of the sparseness of the system (see Smith & Booker 1991).

The FDA nodes and finite-element corners for this test are identical, and are listed in Table 1. The boundary conditions on the distant edges of the model are also conceptually the same for both algorithms. However, PW2D solves for 2-D 'secondary' perturbations to the analytic solution for fields in a 1-D host (taken to be the structure at the left edge of the model), while FWD2D solves directly for the total fields. A property of the secondary-field approach is that it always converges to the analytic 1-D solution as the two-dimensionality of the model vanishes. The total-field approach will only do so if the model has been adequately discretized in the vertical direction. If the secondary fields are substantially smaller than those in the 1-D host, one should expect higher absolute accuracy for PW2D, or alternatively less stringent requirements on numerical precision or model discretization. When the model is strongly 2-D and the secondary fields become comparable to the total fields, the accuracy of the total and secondary-field approaches should be similar.

Fig. 3 shows surface values of the TE responses, ρ_{xy} and ϕ_{xy}, as a function of position for frequencies at which the skin depth is smaller and larger than the width of the valley. The

Table 1. Nodes and finite-element corners for model (a) in Fig. 2. The vertices of the valley are at $(y, z) = (-500, 0), (-300, 200), (300, 200), (500, 0)$. Units are metres.

Horizontal

-50000	-30000	-20000	-12000	-8000	-5000	-3000	-2000	-1500	-1000
-800	-700	-650	-600	-550	-525	-510	-500	-490	-475
-450	-400	-350	-300	-275	-260	-250	-240	-225	-200
-150	-100	-50	0	50	100	150	200	225	240
250	260	275	300	350	400	450	475	490	500
510	525	550	600	650	700	800	1000	1500	2000
3000	5000	8000	12000	20000	30000	50000			

Vertical

-100000	30000	-10000	-3000	-1000	-300	-100	-30	-10	0
10	25	50	100	150	200	225	240	250	260
275	300	350	400	450	500	600	700	800	900
1010	1131	1264	1411	1572	1749	1944	2158	2394	2653
2938	3252	3597	3977	4395	4854	5360	5916	6528	7200
7940	8754	9650	10635	11718	12910	14221	15663	17249	18994
20914									

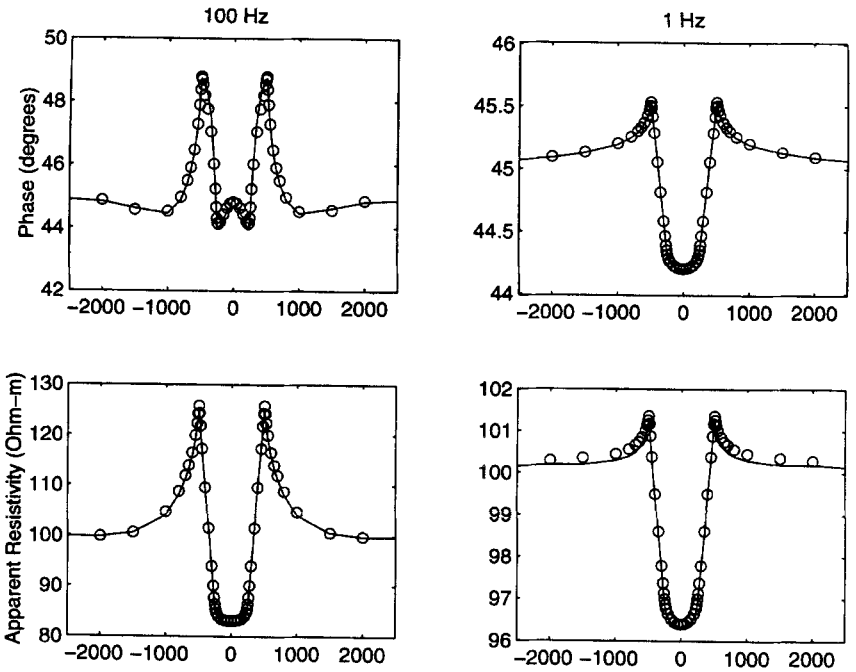

Figure 3. Surface values of the TE phase (top) and apparent resistivity (bottom) for 100 Hz (left) and 1 Hz (right) for the trapezoidal valley of Fig. 2(a). Finite-element responses are plotted as open circles at the horizontal position of each element corner on the Earth–air interface. FDA results have nodes at the same positions and are shown as solid curves. The differences between the responses are much less than 1 per cent in resistivity of 0.29 degrees in phase. The small (0.2 per cent) systematic offset noticeable between the resistivities at 1 Hz is believed to be a result of the secondary and total-field approaches of the two codes (see text).

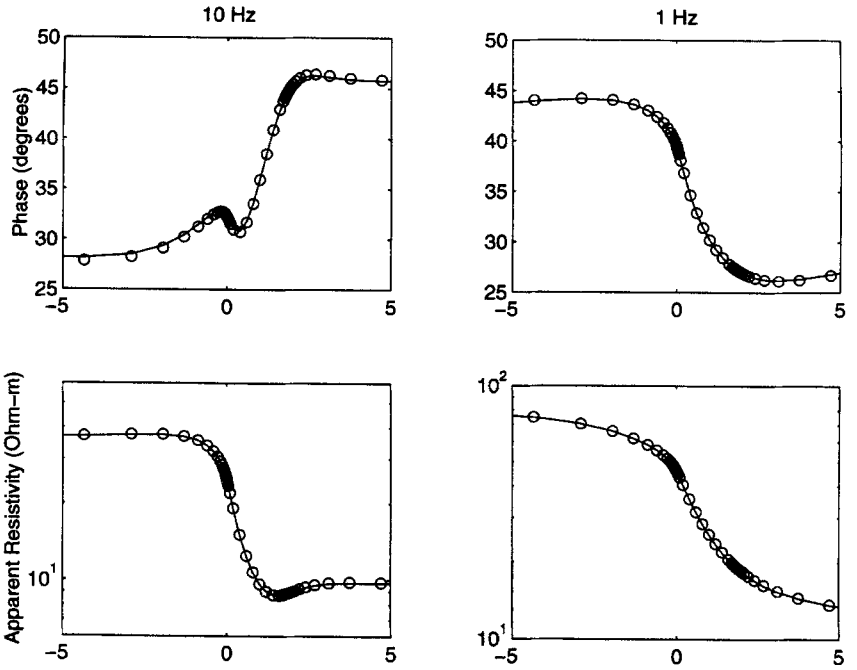

Figure 4. TE responses at 10 Hz (left) and 1 Hz (right) for the model with an internal sloping interface shown in Fig. 2(b). Finite-element responses are plotted as open circles at the horizontal position of each element corner on the Earth–air interface. FDA results have nodes at the same positions and are shown as solid curves.

responses use the electric and magnetic field calculated in the horizontal direction for both methods. Wannamaker, Stodt & Rijo (1986) discussed measuring the magnetic field in the direction parallel to a sloping surface and in the horizontal, and concluded that the most convenient choice for a practical MT experiment, horizontal, minimizes so-called 'static shift' effects of topography. The two methods agree to much better than 1 per cent in apparent resistivity and to better than the equivalent difference of 0.29 degrees in phase. The small, but noticeable offset between the apparent resistivities at 1 Hz

Table 2. Nodes and finite-element corners for model (b) in Fig. 2. The negative vertical values are in the air and are used only for the TE mode. The vertices of the shallow internal interface are at $(y, z) = (0, 100), (1800, 1000)$. Units are metres.

Horizontal

-100000	70000	-50000	-35000	-25000	-20000	-14621	-9756	-6512	-4350
-2908	-1947	-1306	-879	-595	-405	-278	-194	-138	-100
-75	-50	-30	-10	0	10	30	50	100	200
400	600	800	1000	1200	1400	1600	1700	1750	1770
1790	1800	1810	1830	1850	1875	1900	1938	1994	2078
2205	2395	2679	3106	3747	4708	6150	8312	11556	16421
23720									

Vertical

-100000	30000	-10000	-3000	-1000	-300	-100	-75	-50	-25
0	25	50	75	95	100	105	115	125	150
200	300	400	500	600	700	800	900	950	975
985	995	1000	1005	1015	1025	1050	1100	1200	1300
1500	1800	2100	3000	3500	4000	4500	4700	4900	5000
5100	5200	5400	5620	5862	6128	6421	6743	7097	7487
7916	8387	8906	9477	10105	10795	11554	12390	13309	14320
15432	16655	18001	19481	21109					

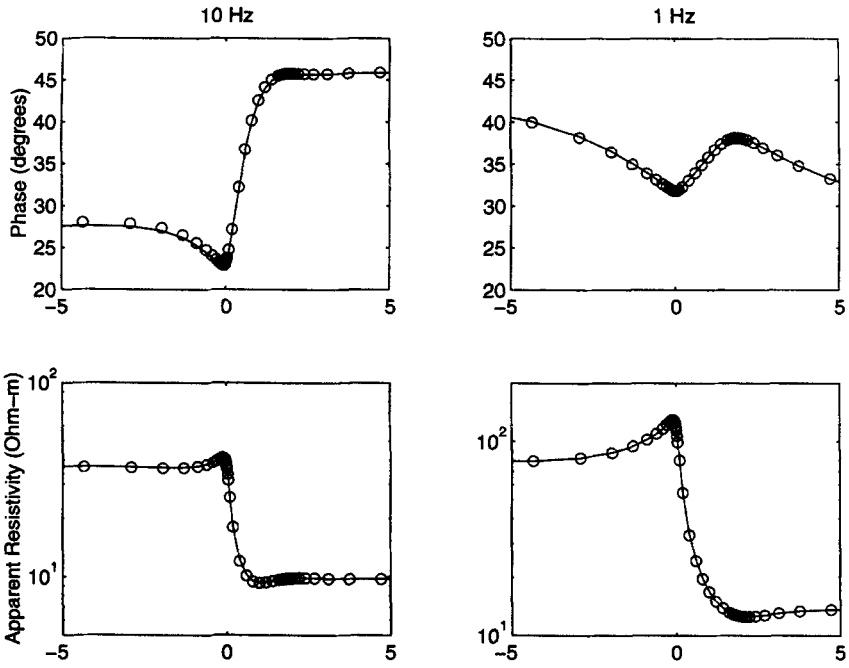

Figure 5. TM responses at 10 Hz (left) and 1 Hz (right) for the model with an internal sloping interface shown in Fig. 2(b). Finite-element responses are plotted as open circles at the horizontal position of each element corner on the Earth–air interface. The FDA results have nodes at the same positions and are shown as solid curves.

persists to large horizontal distances, where PW2D converges to 100 o m and FWD2D converges to 99.88 o m. This offset is actually slightly larger at 100 Hz, but is masked by the larger amplitude of the anomaly. It is a consequence of the difference between the total and secondary-field approaches and will be discussed in more detail in the next example. Our FDA results are in far better agreement with the finite-element results than the agreement between the transmission-line results of Ngoc (1980) and finite-element results for a similar model reported by Wannamaker *et al.* (1986).

4.2 Discrete FDA versus finite elements for an internal sloping boundary

The model of Fig. 2(b) has an internal sloping interface, and Table 2 gives the FDA nodes and finite-element corners. Fig. 4 compares the surface TE responses at frequencies where the skin depth is smaller than or larger than the thickness of the surface layer on the right side of the model. Fig. 5 compares TM responses (ρ_{xy} and ϕ_{xy}) using the discrete TM(d) FDA of eq. (11) at the same frequencies. This FDA can be used everywhere in the model because the resistivities are constant except at the discontinuities.

The responses are again almost indistinguishable at the 1 per cent (0.29 deg) level. The only obvious difference is a small, systematic bias of the phases at 10 Hz on the left side of the model. These differences are plotted for the full width of the model in Fig. 6. They are almost certainly a consequence of the secondary and total-field approaches and are not a result of the finite-difference or finite-element approximations. Both codes estimate the vertical derivative at the Earth–air interface in eqs (1b) or (2b) from a parabolic fit to three field points that do not straddle the discontinuity of the second derivative at the Earth–air interface. For TE, the field points are in the air, where a parabola is a better approximation to the solution than it is in the Earth. For TM, the points must be in the Earth. For the total field, this results in error terms that are usually opposite in sign for TE and TM and slightly larger for TM. However, PW2D needs to apply the numerical differentiation only to the non-1-D host part of the field, which, by assumption, approaches zero on the left side of the model. Thus the PW2D error terms also approach zero on the left,

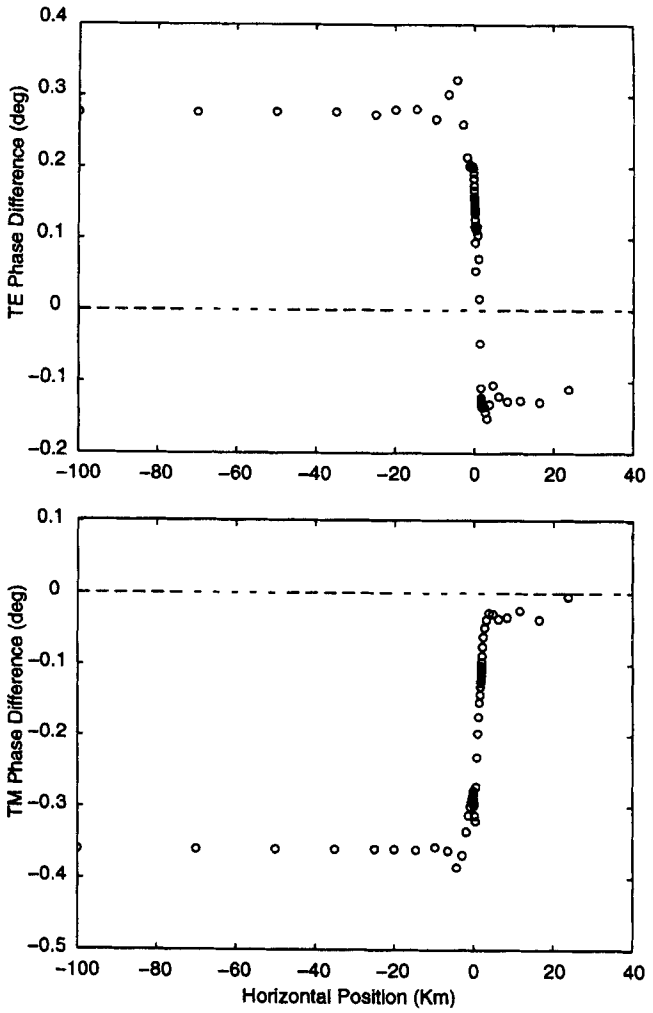

Figure 6. Phase differences between finite-element and finite-difference calculations at 10 Hz for the model with an internal sloping interface shown in Fig. 2(b). The points are plotted at the positions of the finite-difference nodes and the finite-element corners for the full width of the model. A phase difference of ± 0.29 degrees is equivalent to 1 per cent difference in apparent resistivity. The systematic behaviour of these differences is consistent with what is expected between a code that uses total fields and one that uses secondary fields relative to the analytic response of the 1-D structure at the left edge of the model (see text).

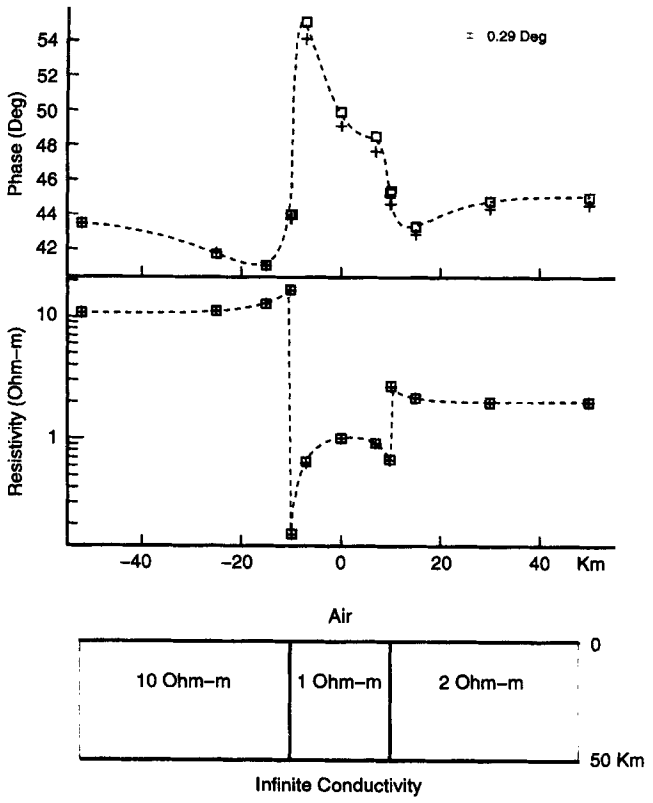

Figure 7. TM responses computed analytically (squares, Weaver *et al.* 1985), with finite elements (crosses, Wannamaker *et al.* 1987) and with FDA TM(d) (dashed lines) at a period of 300 s for the model shown. The model is uniform to infinity outside the central region. Both the finite-element and FDA computations approximate the infinite conductivity of the basement with 10^{10} S m^{-1}. The analytic and finite-element results are computed from Table 1 of Wannamaker *et al.* 1987.

and the observed phase difference is entirely due to the inaccuracy of the 1-D total field. On the right side of the model, the 1-D structure is substantially different from the 1-D host assumed by PW2D, and the secondary fields are a significant fraction of the total fields. Thus the PW2D error terms will also be significant and the observed phase difference is substantially smaller. The accuracy of the 1-D total field can be increased considerably by finer gridding; response differences between the total and secondary field approaches are not evident at 1 Hz.

4.3 Comparison with analytic results when the Galvanic response is large

For the TM mode, continuity of the normal component of an electric current at an interface between media of different conductivities implies charge accumulation on the interface. The 'Galvanic' electric field of these charges does not necessarily disappear as frequency tends to zero and the governing physics changes from diffusion to electrostatics (Poisson's equation). This near-singularity means that computation of the fields from the diffusion equation at frequencies where the Galvanic response is significant may become numerically unstable. Weaver, LeQuang & Fischer (1985) presented an analytic solution for a model consisting of three blocks of differing conductivity overlying an infinitely conducting basement (see Fig. 7). Wannamaker *et al.* (1987) demonstrated the accuracy and stability of PW2D by comparing their responses to these analytic results at 300 s. At this period, the surface units are all more than one skin depth thick, so that induction in the basal infinite conductor is of little importance. Instead, the TM response is strongly influenced by the Galvanic charges on the vertical contacts, which cause large discontinuities in surface apparent resistivity. Fig. 7 extends this comparison to include responses calculated using FWD2D with the TM(d) FDA.

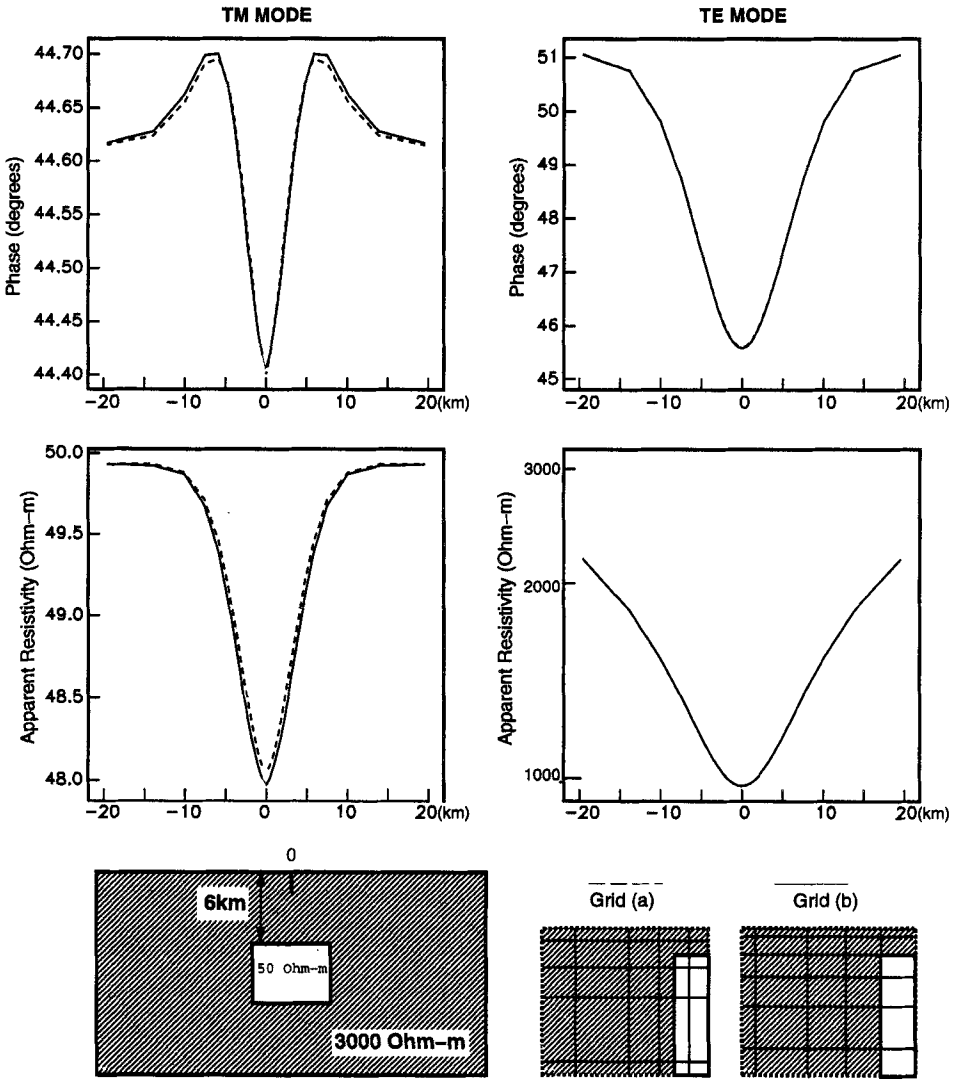

Figure 8. TM (left) and TE (right) responses at 1 Hz for the model shown. Note that the length scales for the model and responses are not the same and that the response scales are different for each mode. The responses were calculated with two different grids: (a) the discrete boundaries of the internal conducting prism pass between the nodes and (b) the nodes lie on the discrete internal boundaries. The TE FDA is the same for both cases, but the effective conductivities near the discrete boundary differ. The TE dashed response of (a) lies within the width of the solid response curve of (b) and cannot be distinguished. The TM(c2) FDA was used for (a) and the TM(d) FDA was used for (b).

FWD2D agrees with the analytical results to better than 1 per cent (0.29 degrees) and the FWD2D phase appears to be in better agreement than is the PW2D phase in the right half of the model. We do not know why PW2D has not performed quite as well as FWD2D in this instance. The grids are very similar, although not identical, and are unlikely to cause this difference. Both numerical models approximate the infinitely conducting basement with a conductivity of 10^{10} S m^{-1}. Differences between the total and secondary-field approaches are also unlikely, because the secondary fields are up to 30 per cent of the total field in the right block and even larger in the centre block. Furthermore, the two numerical codes agree in the left block, where such differences are most likely. Remaining possibilities include the accuracy of the different linear system solvers and the higher-precision arithmetic used by FWD2D (64 versus 32 bits for PW2D).

4.4 Discrete boundaries that do not intersect nodes

Fig. 8 shows the TE and TM responses at 1 Hz for an infinitely long conductive prism in a resistive host. At this frequency, the skin depth in the prism is comparable to its size, while the skin depth in the host is much larger than the depth to the prism. In this situation, the TE response is dominated by current induced in the prism, while the TM response has small, but significant inductive and Galvanic contributions. For both modes, these are strong electric-field gradients near the outer edge of the prism. Responses are shown for a grid in which the discrete boundaries intersect the nodes, and one in which the discrete boundaries lie between the nodes. The TE calculations use the same FDA for both grids, but different effective conductivities at the nodes. The TM calculations use the TM(d) FDA for the discrete boundaries that intersect the nodes and the TM(c2) FDA for the discrete boundaries that do not intersect the nodes.

The TE responses for the two grids are identical within the width of the line, and it is clear that choosing whether or not discrete boundaries intersect nodes is simply a matter of convenience. The two cases give slighty different TM responses, but the difference is much less than 1 per cent (0.29 degrees), and very small compared to the amplitude of the anomaly. Thus, although the non-intersecting case using TM(c2) does not give exactly the same answer as the intersecting case using TM(d), the responses are close enough for most purposes to opt for the simplicity of TM(c2). This is especially true since TM(c2) can also be used in regions of variable ρ away from the discontinuity. In fact, in our experience, increasing the grid spacing near the discontinuity degrades the response accuracy of the non-intersecting case using TM(c2) more slowly than the intersecting case using TM(d). When the grid is sparse due to computer resources or other considerations, non-intersecting discontinuities using TM(c2) often out-perform intersecting discontinuities using TM(d). The currently distributed code for the rapid 2-D inversion of Smith & Booker (1991) uses TM(c2).

4.5 Comparison of the TM FDAs for continuous models

We wish to compare the TM(c1) and TM(c2) FDAs as conductivity gradients increase within a model. To do this, we have developed the suite of four models with successively smoother gradients, as shown in Fig. 9 (m1, m2, m3 and m4), from an originally discrete model (m0). Fig. 10 shows the TM responses at 0.42 Hz for each of the four continuous models.

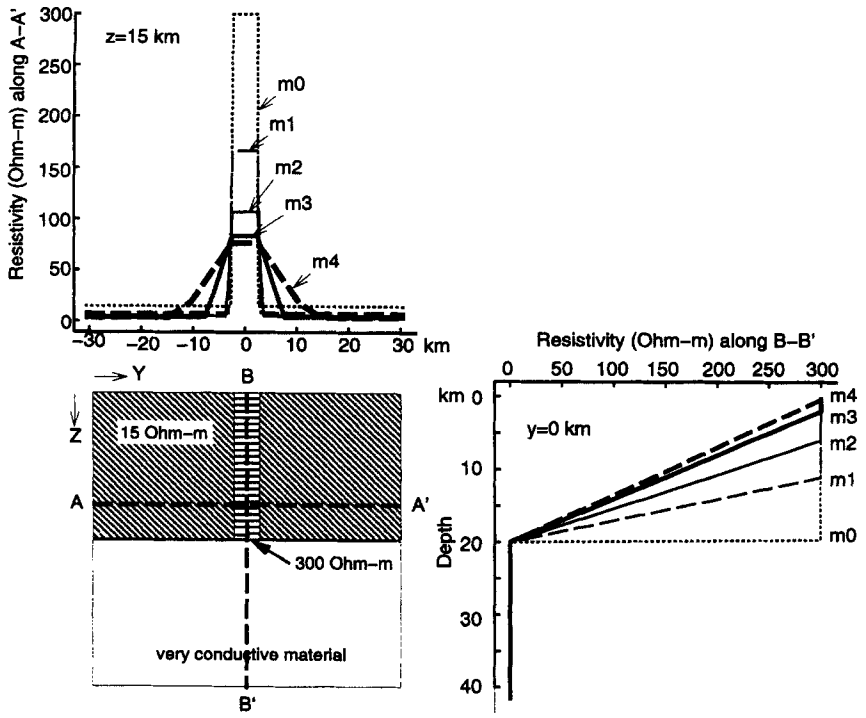

Figure 9. Suite of five models with progressively smaller resistivity gradients. Model m0 is a 5 km wide 300 o m discrete body in a 15 o m horizontal layer. Both overlie a very conductive basement at a depth of 20 km. The subsequent models replace the infinite gradient at the top of the basement and at the vertical edges of the central body with a finite zone of constant resistivity gradient that gets progressively wider from model m1 to m4. This is illustrated by plotting the resistivity along A–A′ at 15 km depth and B–B′ at the middle of the central body.

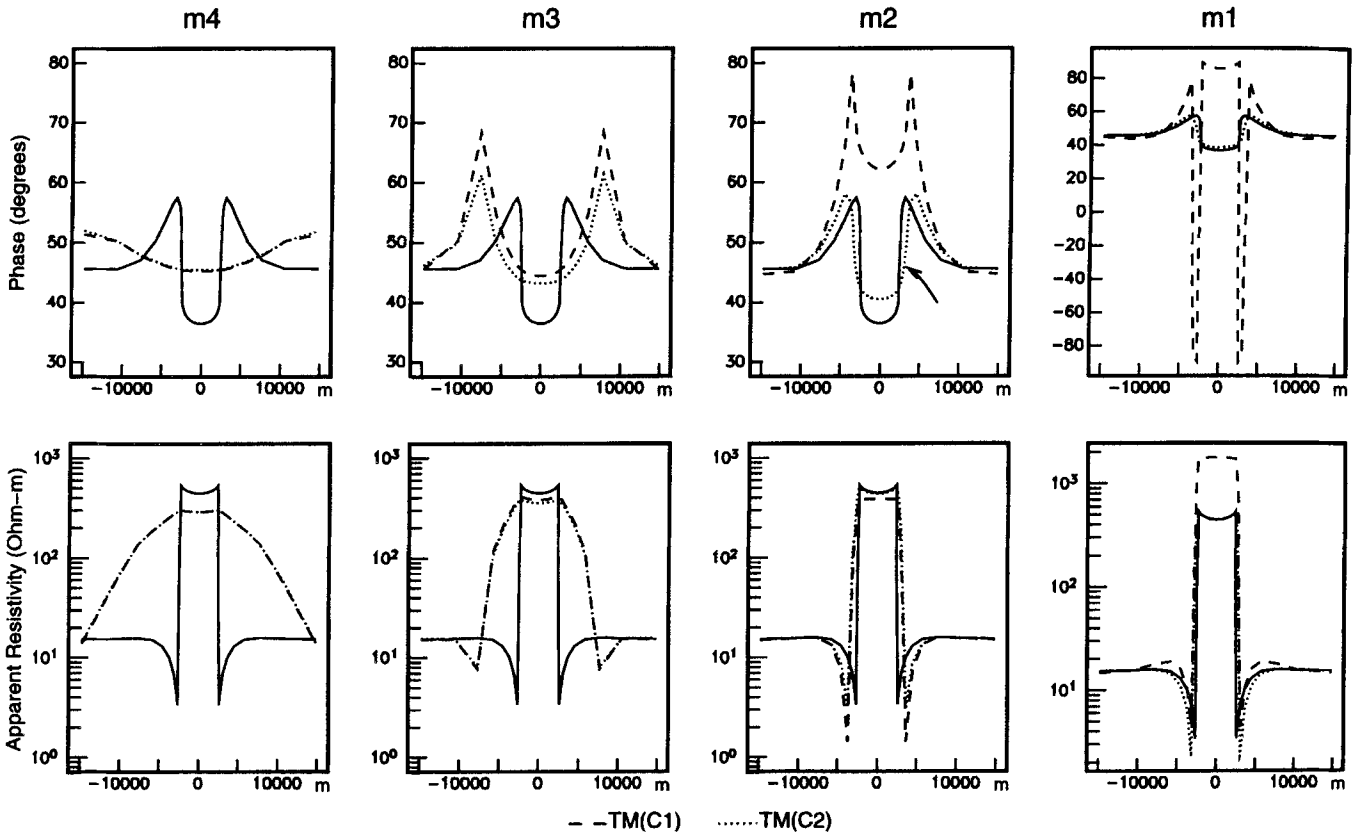

Figure 10. Comparison of TM responses for the suite of models defined in Fig. 9. In all plots, the solid line is the response of the discrete model m0 using the discrete FDA TM(d). The dashed responses are for the continuous FDA TM(c1) and the dotted responses are for the continuous FDA TM(c2). The same nodes are used for all FDAs. When the model gradients are smallest (model m4), TM(c1) and TM(c2) give identical responses. However, as the gradients increase, the TM(c2) responses converge toward the discrete case, while the TM(c1) responses diverge. Note the different vertical scales on the m4 responses.

At this frequency, the skin depth in the 15 o m host is approximately equal to the width of the 300 o m vertical resistive region, and the skin depth in the 300 o m vertical resistive region is approximately equal to the depth to the highly conducting basement. This guarantees strongly 2-D fields with significant contributions to the response from induction in all elements of the model and the Galvanic electric charges on the vertical edges of the resistive region. Responses were calculated using the two continuous FDA TM(c1) and TM(c2) (dashed lines). The response for the discrete model m0 (solid lines), computed with the discrete FDA TM(d), is included in all cases to show how the TM(c1) and TM(c2) solutions evolve as the continuous models approach m0. From left to right, beginning with the smoothest model (m4 in Fig. 9), we see both the TM(c1) and TM(c2) FDAs give essentially identical results. As the model gradient increases, the responses for the two continuous FDAs deviate from one another, particularly in the phase. The TM(c2) response approaches the TM(d) response as the gradients become steeper, while the TM(c1) response diverges from the TM(d) response. For the continuous model with the steepest gradients, TM(c1) required 126 iterations to reduce the numerical residuals sufficiently to suppose that the linear system had been solved, while TM(d) and TM(c2) required only 47 and 34 iterations respectively. This reflects the numerical instability of TM(c1) with steep gradients. We conclude that TM(c2) is as good as TM(c1) when model gradients are small and much better than TM(c1) when the model gradients are high. Thus TM(c2) is clearly preferable.

5 CONCLUSIONS

We have developed finite-difference approximations with which almost any arbitrary discrete boundary can be modelled in a fairly simple and accurate way. For the TE mode, the FDA for the discrete case can be obtained from the FDA for a constant model by simply replacing the conductivity at each node by an 'effective conductivity', which is an appropriately weighted mean of the actual conductivity surrounding each node. The TM mode is more complicated, because the gradient of the resistivity interacts with the gradient of the magnetic field and consequently four 'effective resistivities' must be specified at each node.

These new FDAs can mimic finite-element approximations by allowing discrete boundaries to cut diagonally across mesh cells. In some sense, the new FDAs are actually more flexible than finite elements, because they allow discrete boundaries that do not intersect nodes. They appear to give essentially identical results to finite elements and lead to sparser matrix equations.

We have also presented an FDA for the TM mode when the model is continuous, which gives accurate results when model gradients are high. This FDA even performs well for a

discrete boundary located between nodes in comparison to the TM FDA designed specifically for a discrete boundary running through the nodes.

Finally, we have noted that maintaining computational accuracy with these FDAs requires careful mesh discretization. The grid should be as uniform as possible anywhere that one expects substantial field gradients in order to take advantage of the higher-order accuracy. For practical computation of the appropriate effective conductivities and resistivities at the nodes, the node spacing also needs to be somewhat less than the size of individual discrete bodies or the scale of continuous conductivity gradients. Finally, the grid spacing should be small compared to the scale of the spatial gradients of the fields. Of the order of one-tenth of the local skin depth is recommended near the surface at which MT responses are to be calculated.

ACKNOWLEDGMENTS

We thank Phil Wannamaker and Randall Mackie for thoughtful reviews that substantially improved this paper. This work was supported by the Department of Energy under grants DE-FG06-89ER14064 and DE-FG06-92ER14231 and the National Science Foundation under grants EAR91-18538 and EAR94-18401.

REFERENCES

Adhidjaja, J.I. & Hohmann, G.W., 1989. A finite-difference algorithm for the transient electromagnetic response of a three-dimensional body, *Geophys. J. Int.*, **98,** 233–242.

Brewitt-Taylor, C.R. & Weaver, J.T., 1976. On the finite-difference solution of two-dimensional induction problems, *Geophys. J. R. astr. Soc.*, **47,** 375–396.

Chen, L., Booker, J.R., Jones, A.G., Wu, N., Unsworth, M., Wei, W. & Tan, H., 1996. Electrically conductive crust in Southern Tibet from INDEPTH magnetotelluric surveying, *Science*, **274,** 1694–1696.

Davis, P.J. & Polonsky, I., 1964. Numerical interpolation, differentiation and integration, in *Handbook of Mathematical Functions*, eds Abramowitz, M. & Stegun, I.A., Dept. Commerce, Washington, DC.

Jones, A.G. & Craven, J.A., 1990. The North American Central Plains conductivity anomaly and its correlation with gravity, seismic and heat flow data in Saskatchewan, *Phys. Earth planet. Int.*, **60,** 169–194.

Jones, A.G., Craven, J.A., McNeice, G.W., Ferguson, I.J., Boyce, T., Farquharson, C. & Ellis, R.G., 1993. North American Central Plains conductivity anomaly within the Trans-Hudson orogen in northern Saskatchewan, Canada, *Geology*, **21,** 1027–1030.

Jones, F.W. & Pascoe, L.J., 1971. A general computer program to determine the perturbations of alternating electric currents in a two-dimensional model of a region of uniform conductivity with an embedded inhomogeneity, *Geophys. J. R. astr. Soc.*, **24,** 3–30.

Jones, F.W. & Thompson, D.J., 1974. A discussion of the finite difference method in computer modeling of electrical conductivity structures. A reply to the discussion of Williamson, Hewlett and Tammemagi, *Geophys. J. R. astr. Soc.*, **37,** 537–543.

Mackie, R.L., Madden, T.R. & Wannamaker, P.E., 1993. Three-dimensional magnetotelluric modeling using difference equations—theory and comparisons to integral equations, *Geophysics*, **58,** 215–226.

Mackie, R.L., Smith, J.T. & Madden, T.R., 1994. Three-dimensional electromagnetic modeling using finite difference equations: the magetotelluric example, *Radio Science*, **29,** 923–935.

Ngoc, P.V., 1980. *Magnetotelluric survey of the Mount Meager region of the Squamish Valley (British Columbia)*, Geomagnetic Service of Canada, Earth Physics Branch, Department of Energy, Mines and Resources, Canada, *OF Rep 80-8-E.*

Ogawa, Y. *et al.*, 1996. Electrical conductivity structures of the Appalachian Orogen in the southeastern U.S., *Geophys. Res. Lett.*, **23,** 1597–1600.

Rodi, W.L., 1976. A technique for improving the accuracy of finite element solutions for magnetotelluric data, *Geophys. J. R. astr. Soc.*, **44,** 483–506.

Smith, J.T., 1988. Rapid inversion of multi-dimensional magnetotelluric data, *PhD thesis*, University of Washington, Washington, DC.

Smith, J.T., 1996a. Conservative Modeling of 3-D Electromagnetic fields: I. Properties and Error Analysis, *Geophysics*, **61,** 1308–1318.

Smith, J.T., 1996b. Conservative Modeling of 3-D Electromagnetic fields: II. Biconjugate gradient solution and an accelerator, *Geophysics*, **61,** 1319–1324.

Smith, J.T. & Booker, J.R., 1991. Rapid inversion of two- and three-dimensional magnetotelluric data, *J. geophys. Res.*, **96,** 3905–3922.

Wannamaker, P.E., Stodt, J.A. & Rijo, L., 1986. Two-dimensional topographic responses in magnetotellurics modeled using finite elements, *Geophysics*, **51,** 2131–2144.

Wannamaker, P.E., Stodt, J.A. & Rijo, L., 1987. A stable finite element solution for two-dimensional magnetotelluric modelling, *Geophys, J. R. astr. Soc.*, **88,** 277–296.

Wannamaker, P.E. *et al.*, 1989. Magnetotelluric Observations across the Juan de Fuca subduction system in the EMSLAB project, *J. geophys. Res.*, **94,** 14 111–14 125.

Weaver, J.T., LeQuang, B.V. & Fischer, G., 1985. A comparison of analytic and numerical results for a 2D control model in electromagnetic induction—I. B-polarization calculations, *Geophys. J. R. astr. Soc.*, **82,** 263–278.

Williamson, K., Hewlett, C. & Tammemagi, H.Y., 1974. Computer modelling of electrical conductivity structures, *Geophys. J. R. astr. Soc.*, **37,** 533–536.